Development of High-Strength Fibers from Aliphatic Polyketones by Melt Spinning and Drawing

P. GUPTA,[1] J. T. SCHULTE,[2] J. E. FLOOD,[3] J. E. SPRUIELL[1]

[1] Materials Science and Engineering, University of Tennessee, Knoxville, Tennessee 37996-2200

[2] Shell Chemial Company, Westhollow Technology Center, Houston, Texas 77251-1380

[3] Union Carbide Corporation, Westhollow Technology Center, P.O. Box 4685, Houston, Texas 77210

Received 30 January 2001; accepted 5 February 2001

ABSTRACT: We have investigated the formation of high-strength, high-modulus fibers from four aliphatic polyketone resins. One resin was a perfectly alternating copolymer of ethylene and carbon monoxide, while the other three were terpolymers containing up to 6 mol % propylene. The mechanical properties were measured as a function of processing conditions, and the structures of the filaments were characterized using birefringence, WAXS, SAXS, SEM, and thermal analysis. Fibers formed from all resins develop very high molecular orientations and a microfibrillar structure. Fibers having room temperature tenacities as high as 10 gpd (~1.1 GPa) were obtained. Tensile moduli reached values as high as 120 gpd (~13 GPa). The melting point of the fibers was primarily dependent on the composition of the resin, while the maximum strength and modulus were largely determined by the maximum draw ratio achieved. The maximum draw ratio achieved in the present experiments was greater for the terpolymers than for the copolymer. © 2001 John Wiley & Sons, Inc. J Appl Polym Sci 82: 1794–1815, 2001

Key words: aliphatic polyketones; melt spinning; drawing; fiber formation; high-strength fiber; fibers; drawing; mechanical properties

INTRODUCTION

The aliphatic polyketones are a class of polymers of great current interest. Due to an excellent combination of chemical resistance and mechanical properties, certain aliphatic polyketones have undergone extensive development as engineering resins in recent years. The specific polymers of interest here are a class consisting of (1) the perfectly alternating copolymer of ethylene and carbon monoxide, and (2) terpolymers in which propylene has been randomly substituted for ethylene in amounts up to 6 mol %. It is worth noting that the perfectly alternating copolymer may also be considered a homopolymer in which the monomer is —(CH_2—CH_2—CO)—. The terpolymers can be represented by the formula: —(CH_2—CH_2—CO)$_n$—(CH_2—CH(CH_3)—CO)$_m$—, and they can also be considered random copolymers.

These polymers are high melting point, semicrystalline materials. Although they have excellent hydrolytic stability, they can undergo aldol condensation reactions that lead to cross-linking and viscosity buildup during long exposures in the melt state.[1] Consequently, it is necessary to prevent long exposure to temperatures at which

Correspondence to: J. E. Spruiell.

Journal of Applied Polymer Science, Vol. 82, 1794–1815 (2001)

the polymers are molten. This makes it necessary to use caution when melt processing these materials. For this reason, and the potential for producing very high strength fibers, an early study investigated solution (gel) spinning[2] as a technique for producing fibers from the perfectly alternating copolymer. The fibers produced by solution spinning and drawing were also characterized in detail,[2–4] and they exhibited excellent tensile strength and initial tensile modulus. More recent work has shown that, with appropriate precautions, melt spinning is feasible,[5–7] and, due to its favorable economics, melt spinning is generally preferred over solution spinning. However, no prior study has documented the structure and properties of melt spun and drawn fibers.

In the present article we report the structure and properties of aliphatic polyketone fibers produced by melt spinning and drawing techniques. Three different compositions (amounts of propylene) were studied. For one composition, two different molecular weight resins were examined.

EXPERIMENTAL

Materials

The polymers used in this experiment were prepared and supplied by Shell Chemical Company. There were four grades:

1. A low molecular weight terpolymer (TLMW): A 1.1 LVN, nominal 60 melt flow, 220°C melting point terpolymer containing about 6 mol % propylene with a nominal M_w of 40,000 g/mol and polydispersity index of 2.84.
2. A higher molecular weight terpolymer (THMW): A 1.5 LVN, nominal 15 melt flow, 220°C melting point terpolymer (~6 mol % propylene) with a nominal M_w of 60,000 g/mol and polydispersity index of 3.0.
3. A higher melting point terpolymer (THMP): A 1.5 LVN, 240°C melting point terpolymer with lower propylene content (about 3.5 mol %) than the other terpolymer materials with a nominal M_w of 60,000 g/mol and polydispersity index of 3.1.
4. A low molecular weight copolymer (CLMW): A 1.2 LVN, nominal 60 melt flow, 255°C melting point copolymer with a nominal M_w of 40,000 g/mol and polydispersity index of 3.1.

Melt Spinning

The key requirement for successful melt spinning of the aliphatic polyketones is to keep the residence time as short a possible. For example, Kormelink et al.[5] have shown that the 220°C melting point terpolymer (6 mol % propylene) should be extruded with a melt temperature below 260°C to avoid excessive viscosity buildup due to crosslinking. Residence times as long as 30 min can be tolerated at a melt temperature of 240°C, though shorter residence times are recommended. Further, it is important to eliminate stagnant zones in the extruder and spin block so that no polymer remains at temperature for excessive periods.

The present resins were melt spun with equipment meeting the above requirements. Prior to melt spinning the resins were dried for at least 8 h at 80°C. In most cases, a yarn containing 32 filaments was spun (in a few cases there were 64 filaments). The spinneret capillaries were 0.5–0.7 mm in diameter with an L/D ratio of 2/1. The extrusion temperatures of the resins were TLMW—250°C; THMW—255°C; THMP—255°C or 275°C; CLMW—266°C. A screen pack made of 325 mesh stainless steel was used. The take-up velocity was 400 m/min for the CLMW resin and 200 m/min for all other resins.

Drawing

Drawing was carried out using two different types of drawing equipment. In one case the drawing was carried out using a Fincor 2-stage continuous drawing apparatus equipped with three sets of heated rolls. A first stage draw was carried out between the first and second rolls, while a second stage draw (if used) was taken between the second and third rolls.

The temperatures of drawing are shown in Table I. The temperature of the first set of rolls was maintained at values ranging from 110–220°C for the copolymer and 110–190°C for the terpolymers. The temperature of the second set of rolls was held at about 10°C above the temperature of the first set of rolls. The third set of rolls was maintained at room temperature. The first set of rolls was rotated at a linear speed of 8 m/min. The third set of rolls was maintained at a speed that would give the desired total draw ratio. The second roll set was kept at a speed between the other two, usually closer to that of the third set than the first, so that the major part of draw took place in the first draw-zone. Using this technique the

Table I Drawing Conditions Using Heated Rolls

	Drawing Temperatures			DR Range	Roll 1 Speed (m/min)
	T_I (°C)	T_{II} (°C)	T_{III} (°C)		
Copolymer	110–220	T_I + 10	25	3–8	8
Terpolymer	110–190	T_I + 10	25	3–8	8

maximum achievable draw ratio was about eight times (see results given later).

Yarns were also drawn in a single or two-stage continuous oven draw process. Typically, the fibers were drawn five times to eight times in the first draw stage, followed by a second stage designed to reach the final draw ratio. This process allowed higher draw ratios to be obtained for the terpolymers (up to 10.5 times).

The temperature of the fibers was not established precisely for the oven drawn samples. The oven temperature ranged from 210–230°C for the THMW and TLMW filaments, and it was set at 250°C for the copolymer. The oven temperature for the 240°C melting point terpolymer (THMP) ranged from 230–250°C. The fibers were passed slowly through the oven (typical feed rate on first godet was 3.05 m/min). Obviously, the polymers did not reach the oven temperature, as the 220°C melting point polymers would have melted at 230°C. As best that could be determined, the temperature reached by the fibers was about 200–210°C for the THMW and TLMW resins and was somewhat higher for the copolymer (CLMW) and the THMP filaments.

Characterization Techniques

Birefringence

Overall orientation of the filaments was characterized by birefringence. This was measured using an Olympus microscope and a 30-order Berek compensator. Assuming negligible form birefringence, the measured birefringence, Δn, consists of components from the amorphous phase and from the crystalline phase:[8]

$$\Delta n = (1 - X_c)\Delta^o_{am} f_{am} + X_c \Delta^o_c f_c \qquad (1)$$

Here, X_c, is the crystalline fraction, Δ°_{am} and Δ°_c are the intrinsic birefringences for the amorphous and crystalline phases, and f_{am} and f_c are the Hermans' orientation factors for the amorphous and crystalline phases. This equation was used to determine the amorphous orientation factors, f_{am}, from the measured crystallinity, birefringence, and the crystalline orientation factors determined from X-ray diffraction data (see later section). The intrinsic birefringences were estimated from the bond polarizabilities given by Denbigh[9] and Bunn.[10]

X-ray Diffraction

All wide-angle patterns of the fibers were obtained using CuKα radiation. Equatorial diffractometer scans were obtained, in reflection, using a Rigaku diffractometer equipped with a graphite crystal monochromator. These patterns were used to obtain a measure of the relative amount of α and β phases present in the samples. The quantitative results were obtained from measurements of the relative intensity of the 210α and 210β reflections. Based on the assumption that the ratio of calculated 210 peak intensities for these two phases is I°_α and I°_β, the volume fraction of the α-phase is given by

$$V_\alpha = \frac{I_\alpha}{I_\alpha + 0.95 I_\beta} \qquad (2)$$

where I_α and I_β are the measured integrated intensities of the 210α and 210β reflections from the sample.

Flat plate film patterns were obtained using nickel filtered radiation and a specimen to film distance of 35 mm. In a few cases, two-dimensional ξ vs. 2θ patterns were obtained using a Philips diffractometer equipped with a single crystal orienter. These data were used to obtain the unit cell dimensions of phases present and to decide the best way to carry out the measurements of the crystalline orientation factors. The intensity distributions needed to obtain the Hermans' crystalline orientation factors were measured using a Rigaku diffractometer equipped with a fiber goniometer in transmission mode. The method of Wilchinsky[11] was used to compute

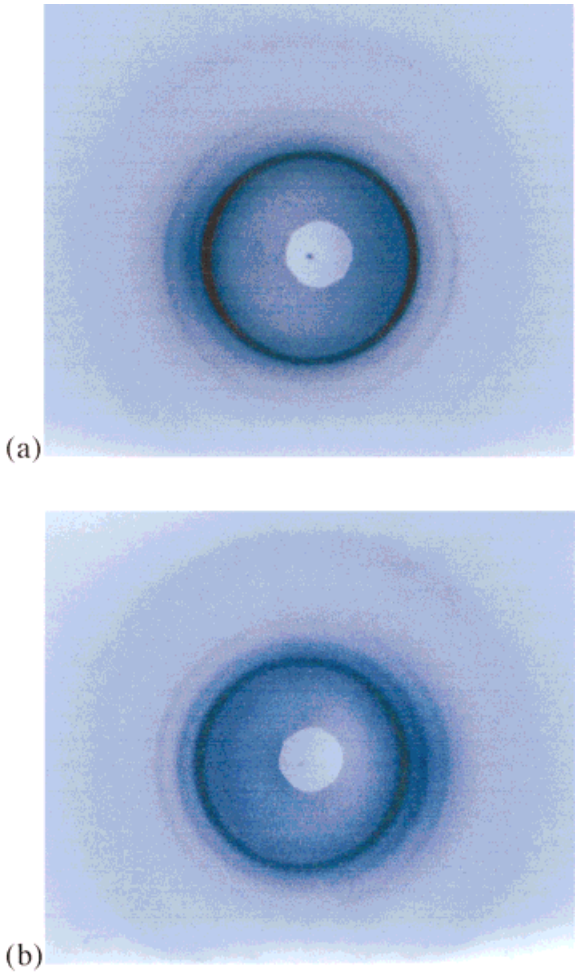

Figure 1 Flat plate X-ray diffraction patterns of as-spun filaments. (a) THMW; (b) CLMW. [Color figure can be viewed in the online issue, which is available at www.interscience.wiley.com.]

the orientation factors from the intensity distributions. The analysis was carried out using the 002 reflection to compute the value of f_c directly. A correction for peak overlap with the tails of the 200 reflection was necessary. This was not a problem for filaments with the high orientation that was found in most of the fibers, but it did cause some error when the orientation factors were less than about 0.7. Only the as-spun fibers were found to have orientation factors that were below 0.7. In this latter case, the orientation factors were computed from the 110 and 210 reflections. In any case, small errors resulting from peak overlap in the as-spun filaments do not affect the conclusions drawn in this article.

Small-angle X-ray scattering (SAXS) measurements were conducted at Oak Ridge National Laboratory's, Center for Small Angle Scattering Research in Oak Ridge, TN.[12] The apparatus has pinhole geometry, rotating anode CuKα X-ray source, a two-dimensional position sensitive detector, and a sample to detector distance of 5.12 m. The scattered intensity was stored in a 64 $\times$ 64 data array. Corrections were made for instrumental background, dark current due to cosmic radiation, electronic noise, and detector nonuniform sensitivity. The primary use of this technique was to measure the long periods found in the fiber samples. These were calculated directly from Bragg's law applied to the position of the first small angle maximum.

Thermal Analysis

The thermal analysis was done with a Perkin-Elmer series seven differential scanning calorimeter (DSC) using Indium, with a melting point of 156.5°C, as the calibration standard. A scan rate of 20°C was used for the determination of melting point and heat of fusion. The % crystallinity of the fibers was computed from the heat of fusion, taking 227 J/g as the heat of fusion for a 100% crystalline terpolymer, and 239 J/g for the copolymer.[13,14] The samples were chopped using scissors and placed into aluminum DSC pans. The sample mass in the pans was kept between 5 and 10 mg.

Tensile Testing

Room temperature tensile testing was done on a Table Model 1122 Instron at a strain rate of 50

Table II Some Basic Characteristics of the As-Spun Filaments

Polymer	Propylene Mol %	Take-Up Velocity m/min	% Crystallinity		Crystalline Orientation Factor
			DSC	Density	
THMW	6	200	35.6	35.0	0.32
TLMW	6	200	36.1	35.2	0.18
THMP	4	200	37.0	—	0.25
CLMW	0	400	45.3	—	0.27

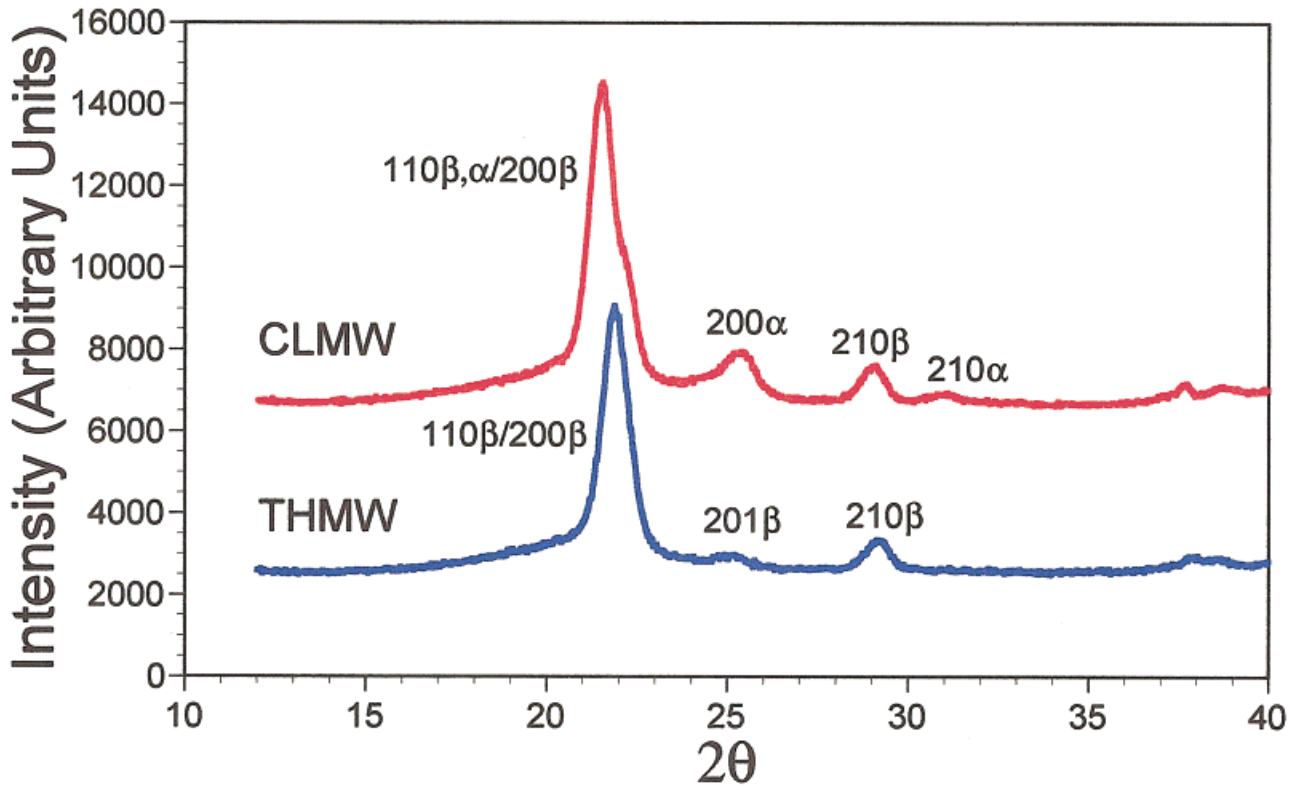

Figure 2 Diffractometer scans of as-spun filaments of (a) copolymer, and (b) the high molecular weight, low melting point terpolymer. Curves are displaced vertically for clarity. [Color figure can be viewed in the online issue, which is available at www.interscience.wiley.com.]

mm/min with a gauge length of 25 mm. A short gauge length was used because specimens at low draw ratios have high elongation to break. Tensile samples of the filament tow were mounted on paper sample holders. The paper holders were prepared with a 25 × 10-mm rectangular window. The fibers were attached to one side of the holder with scotch tape. After mounting the samples between the jaws of the grips, the paper holder strips were cut so that when the test started, the entire load was taken by the fibers.

From the engineering stress–strain curve, the initial tensile modulus (slope of the initial linear part of the curve), tenacity (maximum engineering stress borne by the specimen in units of grams per denier), and % elongation to break were determined.

Sonic Modulus

The sonic moduli of the fiber samples were measured by the technique described by Samuels.[15]

Thermal Shrinkage

Shrinkage upon annealing in an unconstrained (relaxed) state at 165°C for 10 min was calculated from:

$$\%\text{Shrink} = \frac{l_o - l}{l_o} \times 100 \qquad (2)$$

where l is the final length and l_o is the original length. The initial sample length was taken to be 20 cm.

Electron Microscopy

Scanning electron micrographs of peeled fiber samples or of fracture surfaces were prepared using a Cambridge Stereoscan 360 scanning electron microscope. The samples were coated with a thin layer of gold to eliminate sample charging in the beam.

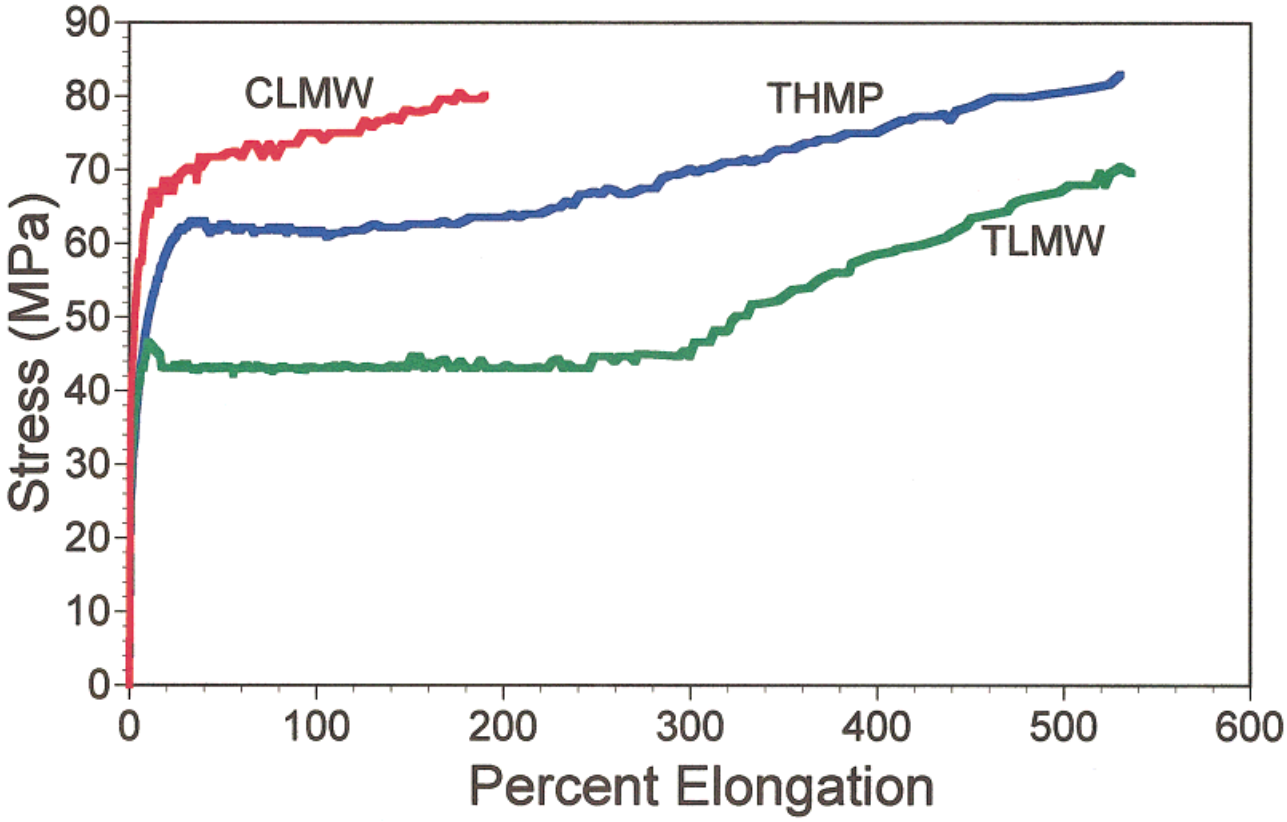

Figure 3 Typical tensile curves for as-spun filaments of selected resins. [Color figure can be viewed in the online issue, which is available at www.interscience.wiley.com.]

RESULTS AND DISCUSSION

Characterization of the Melt-Spun Filaments

Due to the low spinning speeds used to prepare them, the as-spun filaments had very little molecular orientation as is illustrated by the flat plate, wide-angle X-ray diffraction patterns shown in Figure 1. The two patterns shown are representative of as-spun filaments of all four resins. The values of the crystalline orientation functions of the as-spun filaments are shown in Table II. Also shown in Table II are the crystallinities measured via DSC for filaments spun from each of the four resins.

It was shown by Lommerts et al.[3] and Klop et al.[4] that the copolymer usually exists as α-phase at room temperature and undergoes a reversible transition to the β-phase upon heating above 110–125°C. The α-phase has a density about 10% higher than that of the β-phase. Figure 2 shows 2θ scans of as-spun filaments of the copolymer (CLMW) and the high molecular weight terpolymer (THMW). The pattern for the THMW filaments exhibit only the β-phase, and the patterns for the other as-spun terpolymers were essentially identical. The as-spun copolymer filaments did contain some α-phase, but not as much as was expected. This was presumably a result of formation of the β-phase from the melt and retention of this phase to room temperature due to rapid cooling in the spinline. Determination of the relative amount of α and β from the intensities of the 210α and 210β reflections indicated that the crystals present in the as-spun copolymer filaments were only 22 vol % α(23 wt %) and 78 vol % β.

The as-spun filaments of the terpolymers exhibit a typical stress vs. strain curve for ductile thermoplastic polymers. Examples for TLMW and THMP are shown in Figure 3. The terpolymer filaments deformed by the well-known "necking" process. They exhibit a yield point, followed by elongation at essentially constant stress to a "natural draw ratio" corresponding to about 200–300% elongation, followed by a regime in which the stress required to continue deformation increased to a maximum. Fracture occurred after

Table III Mechanical Properties of As-Spun Filaments

Polymer	Tenacity (Tensile Strength)		Initial Tensile Modulus		% Elongation-to-break
	gpd	MPa	gpd	GPa	
THMW	0.639	69.9 ± 5	13.16	1.44 ± 0.04	570 ± 30
TLMW	0.594	65.0 ± 5	13.29	1.45 ± 0.04	565 ± 29
THMP	0.713	78.1 ± 5	13.24	1.45 ± 0.04	540 ± 25
CLMW	0.714	80.9 ± 6	13.2	1.50 ± 0.05	204 ± 30

an elongation of order 500%. The CLMW filament did not exhibit the same type deformation curve nor as much elongation to break as did the terpolymers as illustrated in Figure 3. Table III summarizes the tensile mechanical properties of the as-spun filaments. The properties of these as-spun filaments are similar to the reported tensile properties of injection-molded tensile bars prepared from similar resins,[16] although the reported elongation to break of the tensile bars was lower (300% for terpolymer, 90% for the copolymer). Differences in morphology probably explain the observed differences between the melt spun filaments and the injection molded tensile bars.

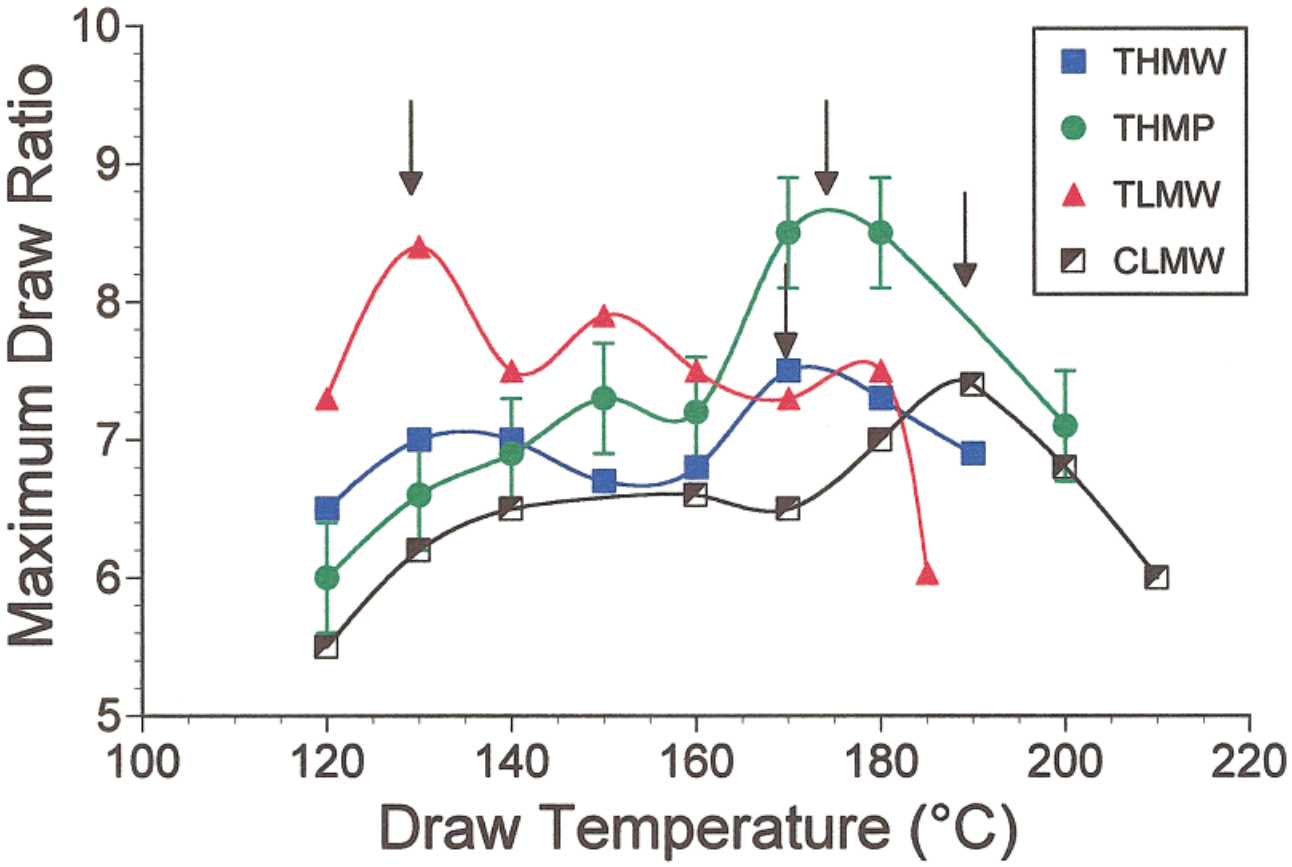

Figure 4 Maximum draw ratio vs. draw temperature for each of the as-spun filaments. Drawing temperature was achieved, in this case, by passing the filaments over heated rolls. Error bars shown only on one set of data for clarity, but are representative of all four cases. [Color figure can be viewed in the online issue, which is available at www.interscience.wiley.com.]

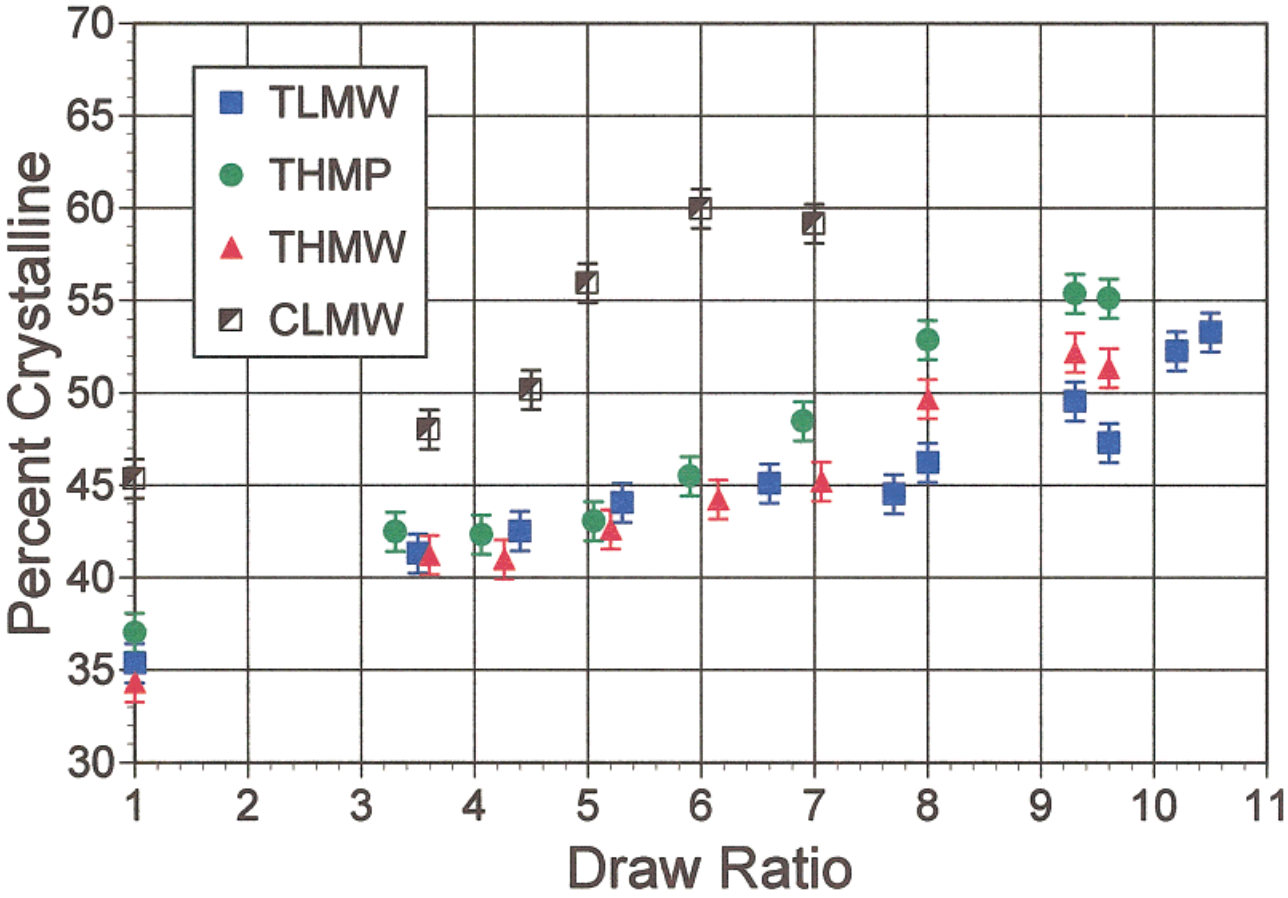

Figure 5 Variation of percent crystallinity with draw ratio for the drawn filaments. Note that the data points at the highest three draw ratios are for oven-drawn fibers, while the lower draw ratios are for fibers drawn over heated rolls. [Color figure can be viewed in the online issue, which is available at www.interscience.wiley.com.]

But the explanation of the lower tensile elongation of the copolymer in comparison to the terpolymers is not clear. Possibilities include: (1) there is a greater level of crosslinking in the copolymer than in the terpolymer, (2) the higher level of crystallinity of the copolymer results in lower elongation, (3) greater thermal degradation of the copolymer, or (4) a combination of the above. We would expect somewhat higher levels of crosslinking in the copolymer due to the fact that it was processed at a higher melt temperature, especially in comparison to the low melting point terpolymers. On the other hand, there is likely less degradation and/or crosslinking in the injection-molded tensile bars than in the melt spun fibers due to shorter exposure time in the melt. The lower elongation of the copolymer tensile bars compared to that of the melt spun filaments seems to argue in favor of some other explanation such as the higher initial crystallinity or some other morphological effect causing the lower elongation of the copolymer. In any case, the high elongation-to-break of the terpolymers suggests that these filaments may be drawn to substantial draw ratios.

Studies of the Drawing Process

As noted above, two major processes were used to continuously draw the as-spun filaments and generate high strength fibers. Preliminary experiments[6] were also carried out using batch drawing of the THMW and TLMW filaments. These preliminary batch-drawing studies involved very slow drawing at a series of temperatures in a hot air oven in a manner similar to a high temperature tensile test. These preliminary studies showed that, under these slow drawing conditions, the maximum draw ratios for the as-spun THMW and TLMW filaments increased from

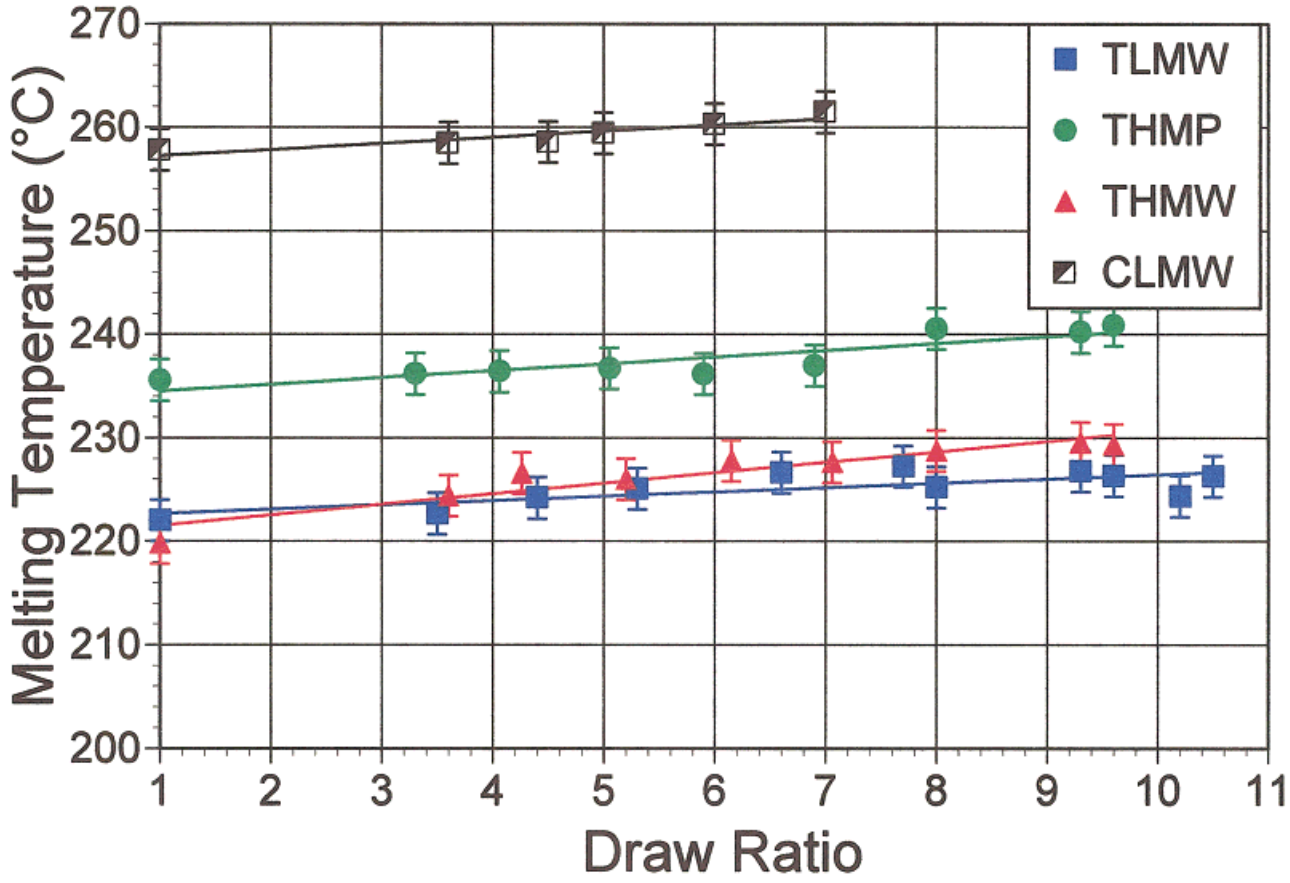

Figure 6 Melting point measured by DSC as a function of draw ratio. [Color figure can be viewed in the online issue, which is available at www.interscience.wiley.com.]

about eight times at 130°C to about 15 times at 180°C.

The continuous roll drawing technique in which the filaments were heated by passage over heated rolls produced the results shown in Figure 4 for the maximum draw ratios of the various resins as a function of temperature. As expected, these values were lower than observed in the case of batch drawing. These results showed that, under these drawing conditions, maximum draw ratios were about 7.5–8.5 times for all four resins studied. In Figure 4 an arrow indicates the optimum draw temperature for each resin. Although each resin exhibited an optimum drawing temperature that increased as the melting point of the polymer increased, all resins could be drawn to draw ratios greater than six times over a fairly wide range of temperatures. This indicates that a fairly wide processing window exists for these resins.

The continuous oven-drawing technique can be considered to be a combination of the best features of batch drawing and continuous drawing over heated rolls. This technique allowed draw ratios as high as 10.5 times to be achieved in a continuous process for the terpolymers. The samples were typically drawn about five to eight times in the first stage draw, followed by a second stage draw to achieve the final draw ratio. Maximum draw ratios for the copolymer were not as high (eight times). The reason for this appears to be related to the cause of the lower tensile elongation of the as-spun filaments described above. As in the above case of elongation of the as-spun filaments and tensile bars, we are not certain at the present time whether crosslinking, higher initial crystallinity, or some other factor causes this result. It is likely, however, that the copolymer filaments may have a higher level of crosslinking or degradation due to exposure to higher temperatures during spinning as described above in discussing the elongation to break of the as-spun filaments. The difficulty of melt processing the copolymer by extrusion techniques due to

crosslinking at the extrusion temperature was mentioned by Ash et al.[1] and by Kormelink et al.[5]

Characterization of Drawn Fiber

Melting Temperature and Crystallinty

Figure 5 shows the variation of % crystallinity with the draw ratio. The crystallinity was calculated from the heat of fusion as discussed previously. The samples all show an increase of crystallinity with increase of draw ratio. The change is rather marked between the as-spun samples and the drawn samples, even at relatively low draw ratios. It should be further noted that there is a sudden increase in crystallinity at the higher draw ratios (last three data points for each resin). This is associated with the switch from drawing over heated rolls at the low draw ratios to oven drawing at the high draw ratios. This effect is presumably caused by the ability to draw at higher temperatures in the oven drawing process. The filaments drawn over heated rolls were all processed at the optimum temperature for each resin shown in Figure 4; these drawing temperatures are all substantially less than those used in the oven drawing technique.

The experimental melting temperatures also increased slightly with increase in draw ratio, as shown in Figure 6. However, the most significant factor affecting the melting temperature is the composition of the resin.

Crystal Structure and Phases Present

Figure 7 shows flat plate X-ray patterns of highly oriented fibers of three of the four resins. The drawing conditions are given in the caption for each fiber. All of the terpolymer samples exhibit the β-structure after drawing, while the CLMW copolymer largely exhibits the α-structure. Indexing of several important reflections is indicated for the THMP and CLMW patterns in Figure 7. Note the absence of the two peaks in close proximity on the first layer line above the equator and the well separated 110α and 200α reflections on the equator of the CLMW pattern. Measurements of the relative intensities of the 210α and 210β reflections as a function of draw ratio indicate that the drawn CLMW fiber consists of about 85% α-phase after a draw ratio of five times. Because the drawing took place well above the α/β transition temperature of about 110–120°C, this probably reflects the fact that the filaments cooled relatively slowly from the draw temperature and largely converted to α-phase during the cool down.

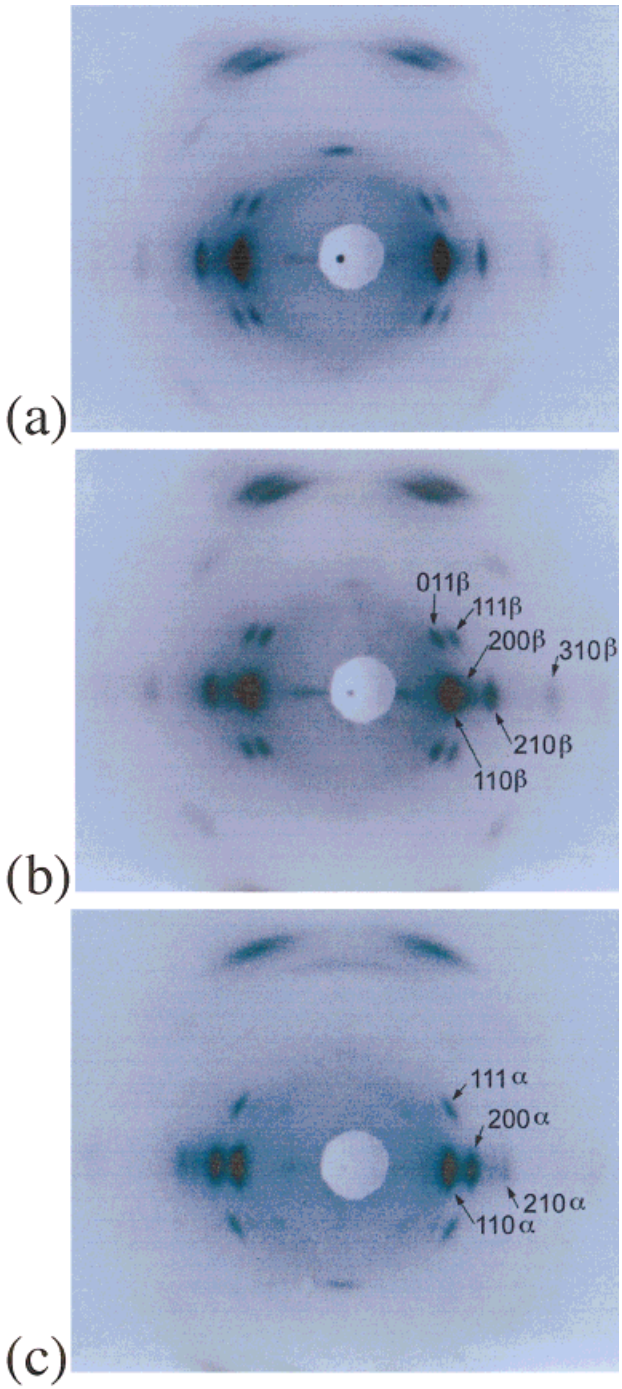

Figure 7 Flat plate X-ray diffraction patterns of highly oriented fibers prepared from selected resins. (a) TLMW, DR = 7.5; (b) THMP, DR = 9.6; (c) CLMW, DR = 7.0. [Color figure can be viewed in the online issue, which is available at www.interscience.wiley.com.]

The unit cell dimensions determined from highly drawn examples of the present melt spun

Table IV Lattice Constants of Drawn Fiber of Aliphatic Polyketones

Investigator (Reference)	Mol % Propylene	Phase	Fiber/ Process	Lattice Constants (Å)			Cell Area (Å)^2	Cell Volume (Å)^3
				a	b	c	$a \times b$	
Present	6	β	TLMW	8.12	4.77	7.59	38.7	294.0
Present	6	β	THMW	8.14	4.76	7.59	38.7	294.1
Present	4	β	THMP	8.04	4.75	7.58	38.2	289.5
Present	0	α	CLMW	6.91	5.13	7.60	35.4	269.4
Klop (4)	5	β	Sol. spun	8.05	4.75	7.61	38.2	290.7
Klop (4)	3	β	Sol. spun	7.96	4.78	7.59	38.0	288.8
Klop (4)	0	α	Sol. spun	6.87	5.12	7.60	35.2	267.3
Lommerts (3)	0	α	Sol. spun	6.91	5.12	7.60	35.4	268.9

and drawn fibers are given in Table IV. They are compared to unit cell dimensions determined by Klop et al.[4] and Lommerts et al.[3] from solution spun fibers prepared from similar aliphatic polyketone resins. It is clear that the present lattice constants are in close agreement with the earlier work of these two references. Thus, the phases formed in the present melt-spun and drawn fibers are equivalent within experimental error of those found earlier for solution spun and drawn fibers. In addition to the formation of the α-phase in the copolymer, it should be noted that there is a

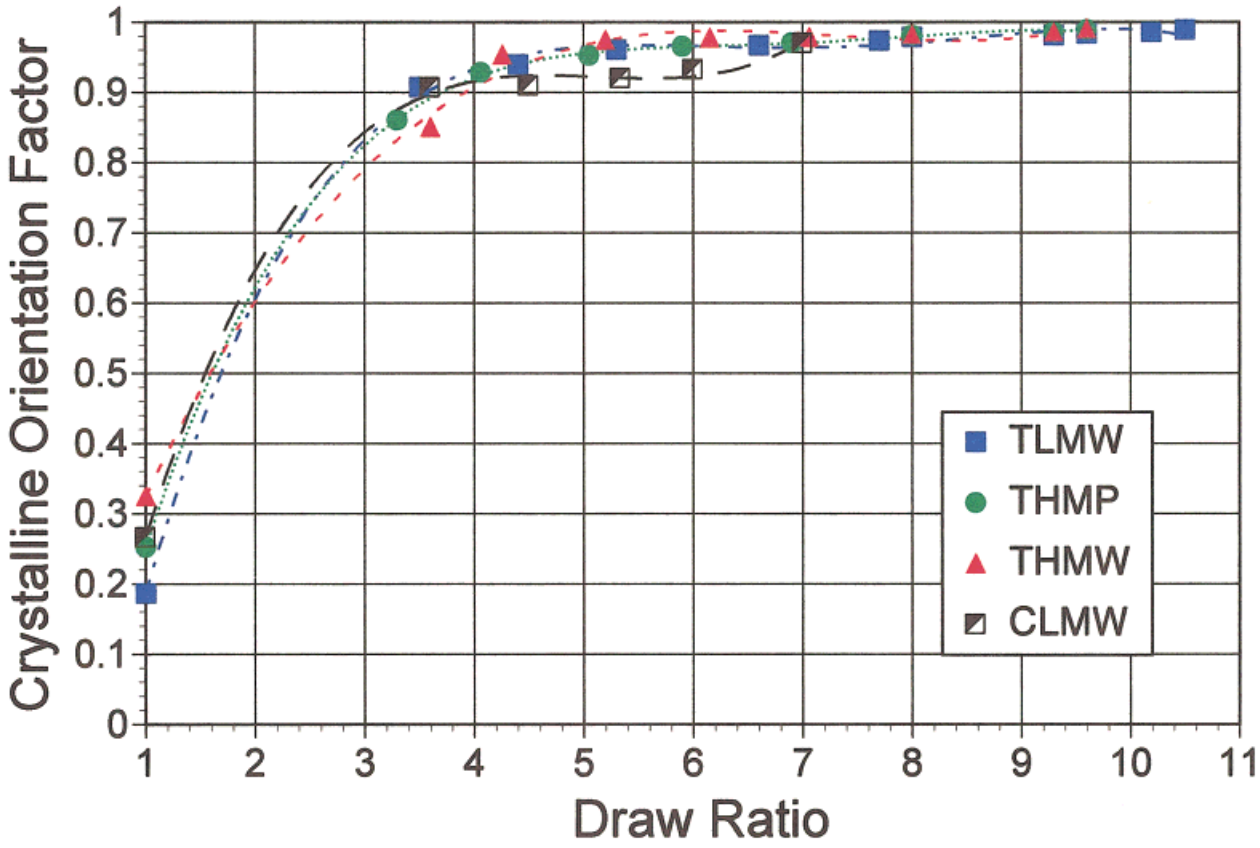

Figure 8 Crystalline orientation factor as a function of draw ratio. [Color figure can be viewed in the online issue, which is available at www.interscience.wiley.com.]

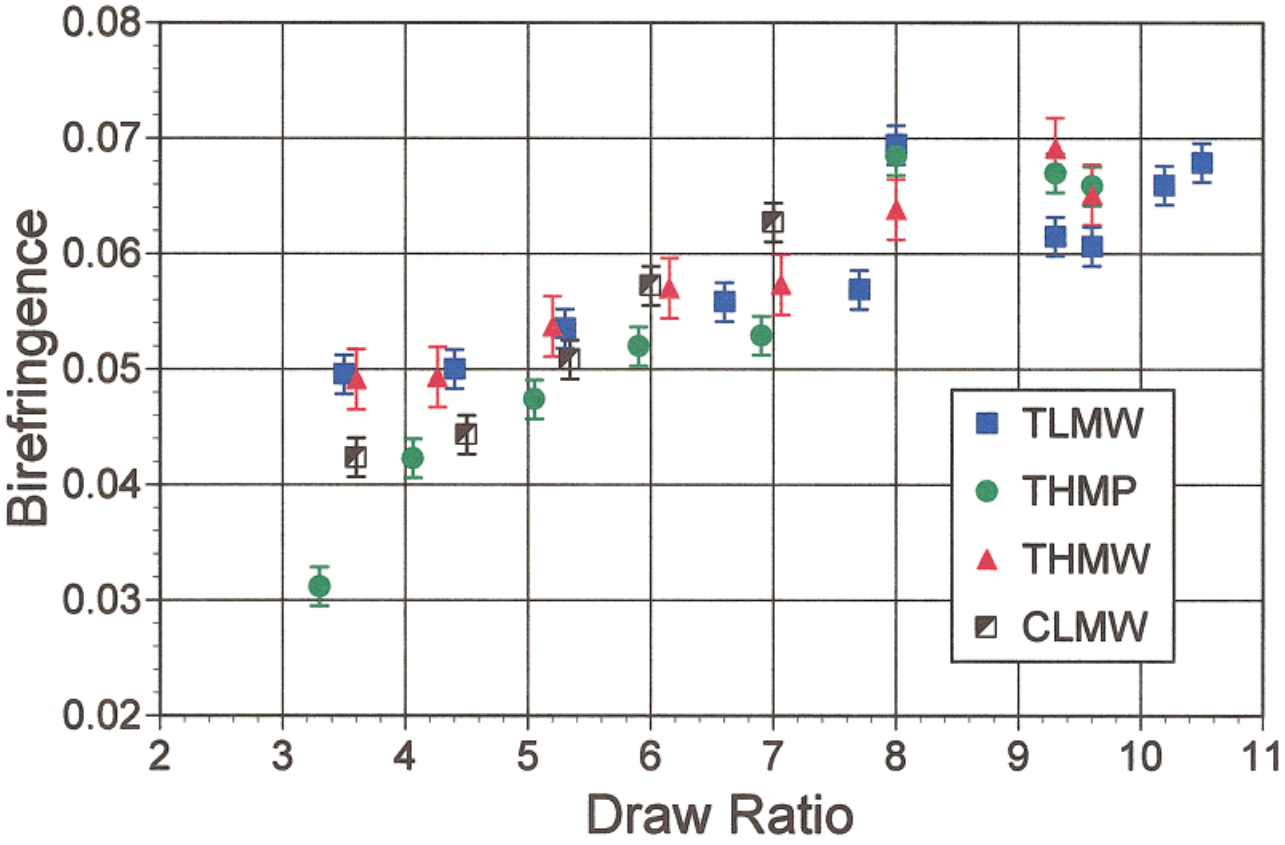

Figure 9 Birefringence as a function of draw ratio. [Color figure can be viewed in the online issue, which is available at www.interscience.wiley.com.]

change in the lattice constants of the β-phase with change in propylene content in the polymer. Klop et al. interpreted this change as evidence that the methyl groups on the propylene are incorporated into the lattice as defects. It seems reasonable to interpret the change in lattice constants in this way, although there is no guarantee that all such propylene units are incorporated in the crystal; some may be rejected.

Development of Crystalline Orientation

The measured crystalline orientation factors for the four polymers are shown in Figure 8 as a function of draw ratio. It is clear from this figure that the crystalline orientation develops rapidly and reaches very high values at high draw ratios. The latter values are clearly consistent with the pinhole X-ray patterns shown in Figure 7. The former is a result of the rapid reorganization of the structure during the necking that occurs during the first stage of drawing. By the time the melt-spun filament is extended to its natural draw ratio (about three times) the reorganization is largely complete, and the majority of crystals are already highly oriented. Continued deformation beyond the natural draw ratio, in either the first stage draw or a second stage draw, further develops and perfects the crystalline orientation. Because the oven-drawn samples reach high draw ratios, they also exhibit very high crystalline orientation.

Birefringence, Amorphous Orientation, and Shrinkage

Figure 9 shows the development of birefringence with draw ratio. The Δn values of the as-spun filaments (DR $=1$) could not be included on the plot due to the fact that the filaments did not pass enough light to allow a measurement of retardation. With increasing draw ratio the birefringence consistently increases. It is clear that the oven-drawn samples achieved higher birefringence than the filaments drawn over heated rolls. This would appear to be a result of both higher crys-

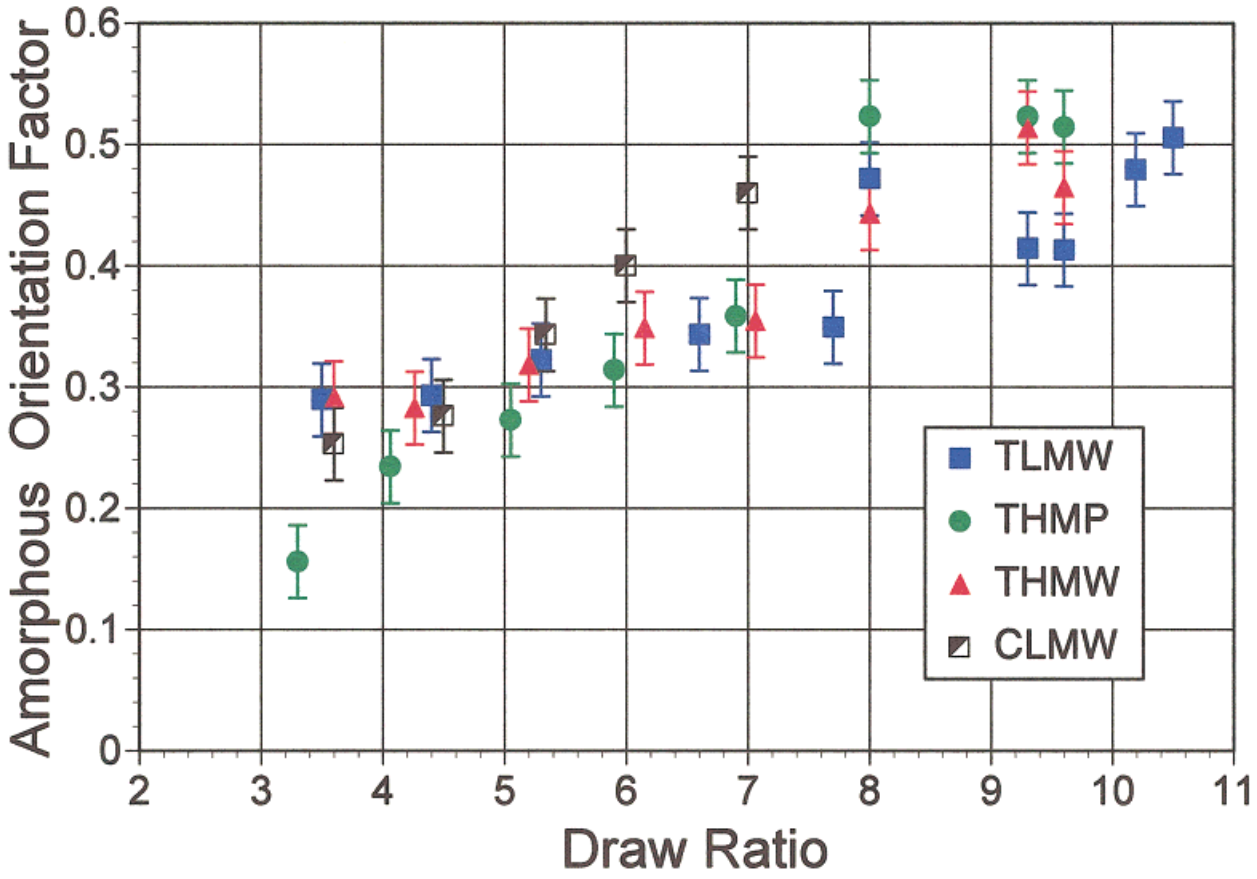

Figure 10 Amorphous orientation factor as a function of draw ratio. [Color figure can be viewed in the online issue, which is available at www.interscience.wiley.com.]

talline orientation and higher amorphous orientation (see below).

Combining the birefringence measurements of Figure 9 with the crystalline orientation measurements of Figure 8 and the crystallinity measurements of Figure 5 through eq. (1) gives the amorphous orientation factors shown in Figure 10. The amorphous orientation increases monotonically with an increase in draw ratio, but at a much slower rate than does the crystalline orientation.

Figure 11 shows the thermal shrinkage of the drawn filaments (after 10 min at 165°C) as a function of the draw ratio. It may be noted that the undrawn (and unoriented) as-spun filaments exhibited zero shrinkage. On drawing at low draw ratios, the shrinkage becomes appreciable, but it decreases with further increase in draw ratio. At first glance this is somewhat surprising in view of the fact that the amorphous orientation continues to increase with draw ratio. However, Figure 5 showed that crystallinity also increased with draw ratio. This suggests that some of the amorphous material is crystallizing during the drawing process and the amount increases with the draw ratio. This would be expected to stabilize and reduce the amount of shrinkage observed. Draw temperature is also important because the oven-drawn samples are drawn at higher temperatures than the roll drawn fibers. Close examination of Figure 11 shows that the decrease in shrinkage is greatest for the THMP and CLMW fibers, and Figure 5 shows that the high draw ratio, oven-drawn THMP and CLMW fibers exhibit substantial increases in crystallinity compared to the lower draw ratio, roll drawn samples.

SEM Photomicrographs

Figure 12 shows SEM photomicrographs of "peeled" THMW fibers as a function of the draw ratio. These reveal a fibrillar or microfibrillar morphology that becomes more apparent with increase in draw ratio, but can be easily detected at

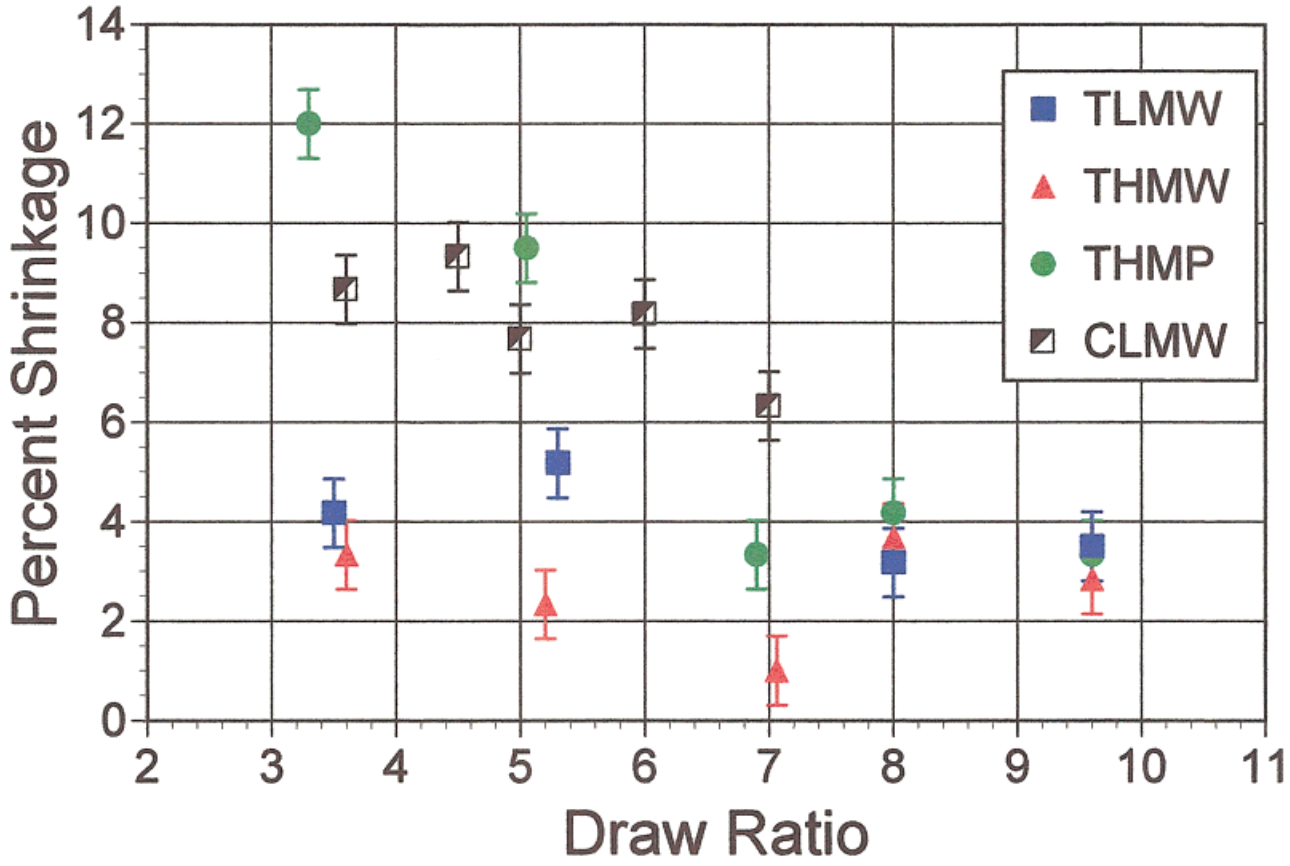

Figure 11 Thermal shrinkage as a function of draw ratio after 10 min at 165°C. [Color figure can be viewed in the online issue, which is available at www.interscience.wiley.com.]

a draw ratio of 3.6. A similar development of microfibrillar morphology is also observed in the fibers produced from the other resins, although the fibrillar structure is somewhat slower to develop in the THMP resin. A possible reason for this might be the higher draw temperature used for the THMP resin compared to the other two terpolymers. The appearance of this fibrillar structure is similar to that which has been observed in other drawn filaments of thermoplastic polymers, such as polyethylene, polypropylene, and others.[17–20]

Photomicrographs of tensile fracture surfaces of highly drawn samples are shown in Figure 13. These also indicate a fibrillar structure. Note that the nature of the fracture tends toward a tail and groove-type fracture. It appears that the fracture initiates at a defect of some type near the fiber surface and then propagates along the microfibril boundaries and gradually works its way along and across the fiber to produce this characteristic failure appearance. This process may also be aided by the presence of elongated voids located between the microfibrils. Evidence for these voids include density decreases due to drawing and the equatorial diffuse scattering observed in the SAXS patterns presented in the next section.

Long Period and Crystallite Size

Contour plots of the SAXS for a few examples of the drawn fibers are shown in Figure 14. At intermediate draw ratios all the filaments exhibited well-developed discrete two-point SAXS patterns. The two-point patterns are interpreted to indicate crystalline lamellae alternating with amorphous regions stacked parallel to the fiber axis. According to the orientation data given above, the c-axis (chain direction) of the crystals are parallel to the fiber axis. At higher draw ratios the contrast that gives rise to the two-point patterns tends to decrease. This is likely due to the fact that the electron density of the amorphous regions in-

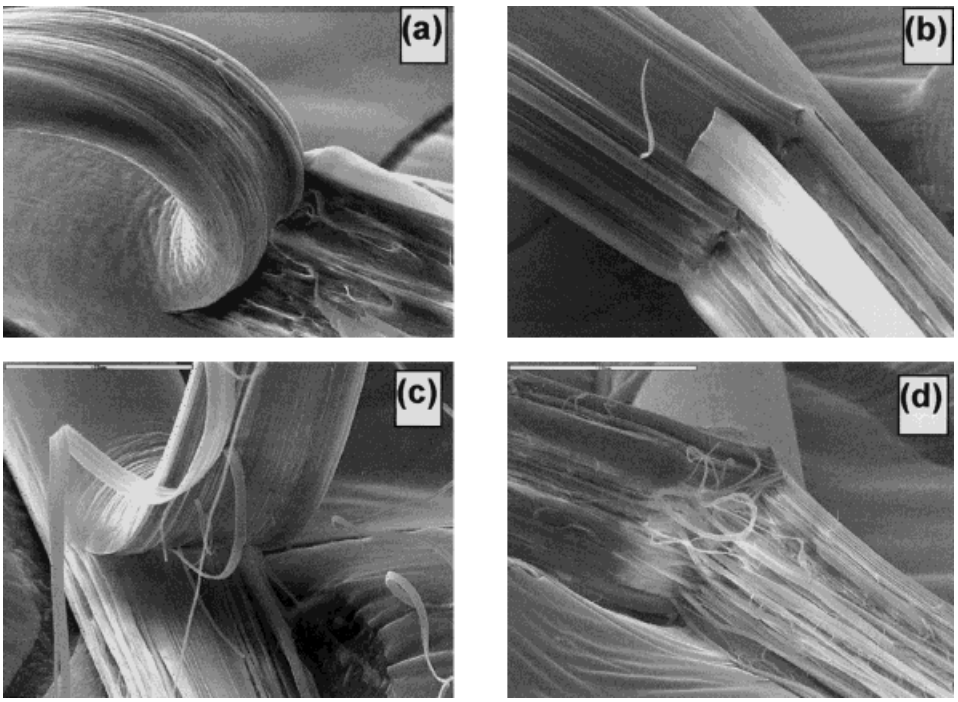

Figure 12 SEM photomicrographs of peeled THMW fibers. (a) DR = 3.6; (b) DR = 5.2; (c) DR = 7.0; (d) DR = 9.6. Magnification markers are 50 μm long.

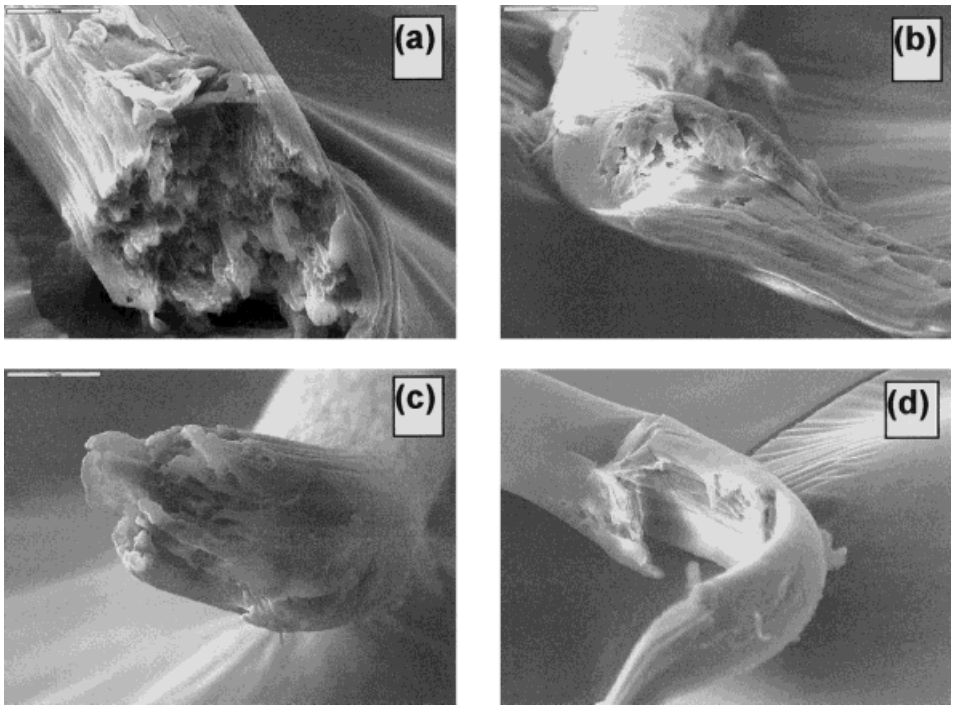

Figure 13 SEM photomicrographs of tensile fracture surfaces of highly drawn aliphatic polyketone fibers. (a) CLMW, DR = 5.0; (b) THMW, DR = 9.6; (c) TLMW, DR = 9.6; (d) THMP, DR = 9.6. Magnification markers are 20 μm long.

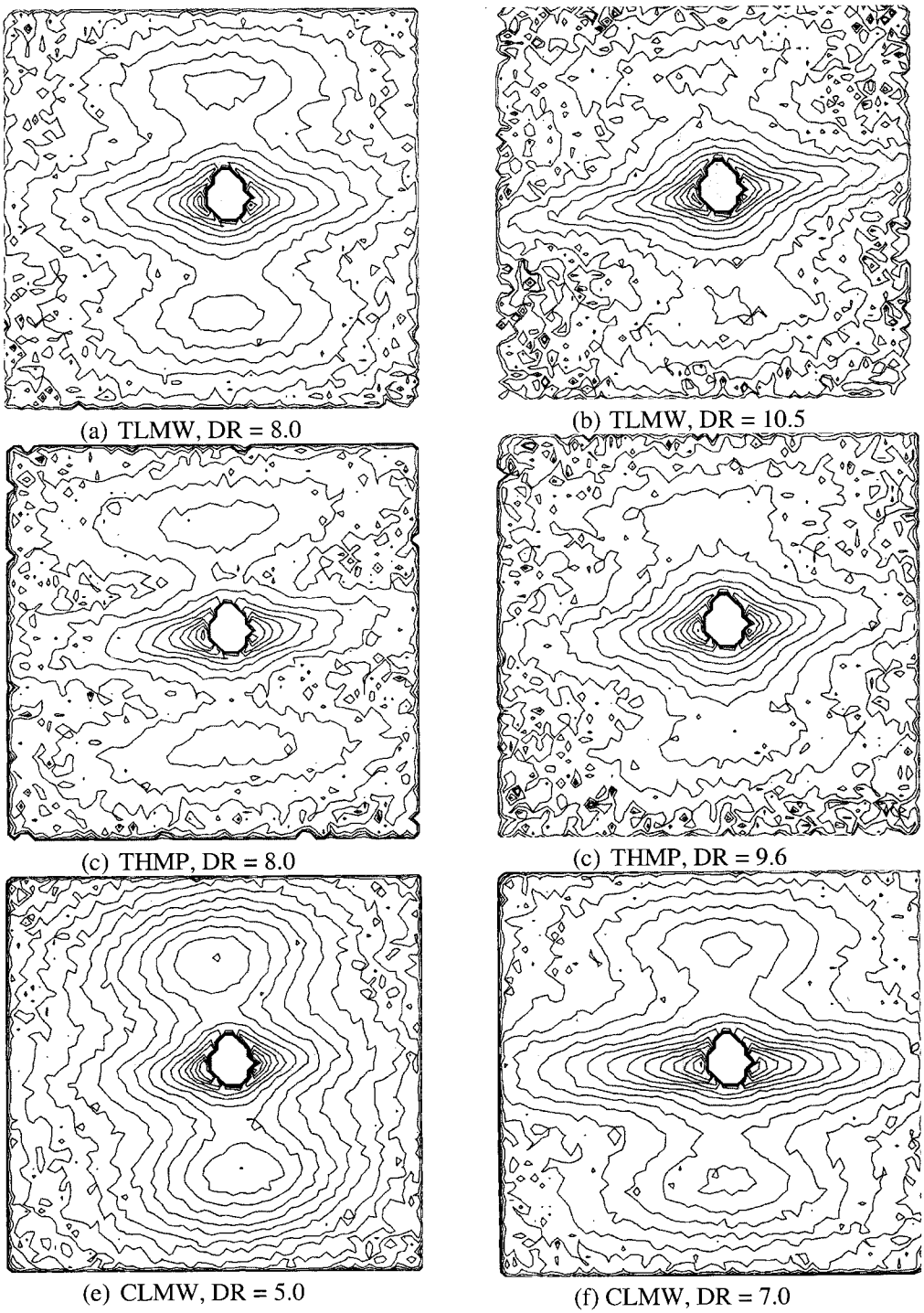

Figure 14 Contour plots showing the SAXS patterns for selected drawn fibers.

creases somewhat with draw ratio and/or perhaps a portion of these regions crystallize. Recall that the crystallinity increases with draw ratio based on DSC heat of fusion measurements. The patterns also exhibited equatorial diffuse scattering. The amount and extent of the diffuse streak increases with the draw ratio. These observations suggest that the fibers gradually develop increasing numbers of elongated voids parallel to the fiber axis as the draw ratio increases.

The long periods for selected fiber samples are given in Table V, along with the lamella thickness

Table V Long Period and Lamellae Thickness of Selected Fibers

Polymer	Condition	DR	Long Period (nm)	Lamellae Thickness (nm)
THMW	As-spun	1	12.93	4.46
THMW	Oven drawn	8	14.93	7.44
THMW	Oven drawn	9.6	14.81	7.63
TLMW	As-spun	1	12.67	4.5
TLMW	Roll drawn	3.5	9.98	4.12
TLMW	Roll drawn	7.7	9.88	4.40
TLMW	Oven drawn	8	16.89	7.84
TLMW	Oven drawn	9.6	16.95	8.21
TLMW	Oven drawn	10.5	15.94	8.53
THMP	As-spun	1	13.42	4.93
THMP	Roll drawn	3.3	11.37	4.78
THMP	Oven drawn	8	15.91	8.72
THMP	Oven drawn	9.6	18.96	10.82
CLMW	As-spun	1	11.27	5.11
CLMW	Roll drawn	3.6	11.91	5.72
CLMW	Roll drawn	7.0	12.04	7.12
CLMW	Oven drawn	5	16.97	9.48
CLMW	Oven drawn	7	15.52	9.27

obtained by multiplying the long period by the crystalline volume fraction for each sample. It is clear that both the long period and the lamella thickness of the oven-drawn fibers are greater than those of the roll-drawn fibers. This indicates that the long period and lamella thickness is a function of the drawing temperature. Increase in draw ratio at the same draw temperature has relatively little effect on either the long period or the lamella thickness. This behavior suggests that the polymer undergoes a recrystallization process during drawing, and the lamellae thickness of the drawn fibers is largely controlled by the temperature at which the recrystallization takes place, i.e., the drawing temperature.

In the case of the highly oriented samples, the lamella thickness can also be estimated from the 2θ X-ray line broadening of the 002 reflection using the Scherrer equation. Measurement on a few of the fibers indicated that these values were consistent with the values obtained from the long period and crystalline fractions.

The crystal size in the direction normal to the (210) planes was also measured for selected samples using the Scherrer equation. This dimension is perpendicular to the fiber axis, and gives an indication of microfibril diameter. These values are shown in Table VI. These results show that the crystal size perpendicular to the (210) planes decreases with increase in draw ratio; this suggests that the microfibril diameters also decrease with draw ratio.

Table VI Crystal Dimensions Perpendicular to the (210) Planes

Polymer	DR	210β Crystallite Size (Å)	210α Crystallite Size (Å)
CLMW	1	144	132
CLMW	3.6	112	114
CLMW	5	—	84
CLMW	7	—	69
THMW	1	137	—
THMW	3.6	84	—
THMW	5.2	75	—
THMW	9.6	73	—
THMP	1	114	—
THMP	3.3	91	—
THMP	5	84	—
THMP	8	70	—

Structure Model of Drawn Fibers

The spherulitic structure of the as-spun filaments is converted to the structure of the drawn fibers by processes that involve disintegration of the spherulites, crystal cleavage, pull-out of chains from the crystals, slip, reorientation, recrystallization and, ultimately, formation of a microfibrillar structure in which the chain axes of the crystals are parallel to the fiber axis and the crystal lamella thickness is determined by the draw temperature. This process has been previously described in the case of other thermoplastic polymers by several investigators, including Peterlin,[21,22] Samuels,[15] Prevorsek et al.,[23] and others.

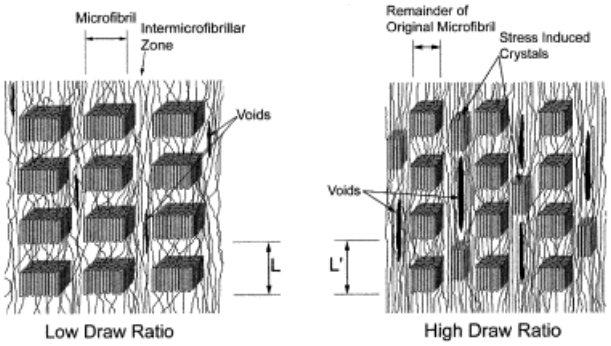

Figure 15 Model of melt spun and drawn aliphatic polyketone fibers.

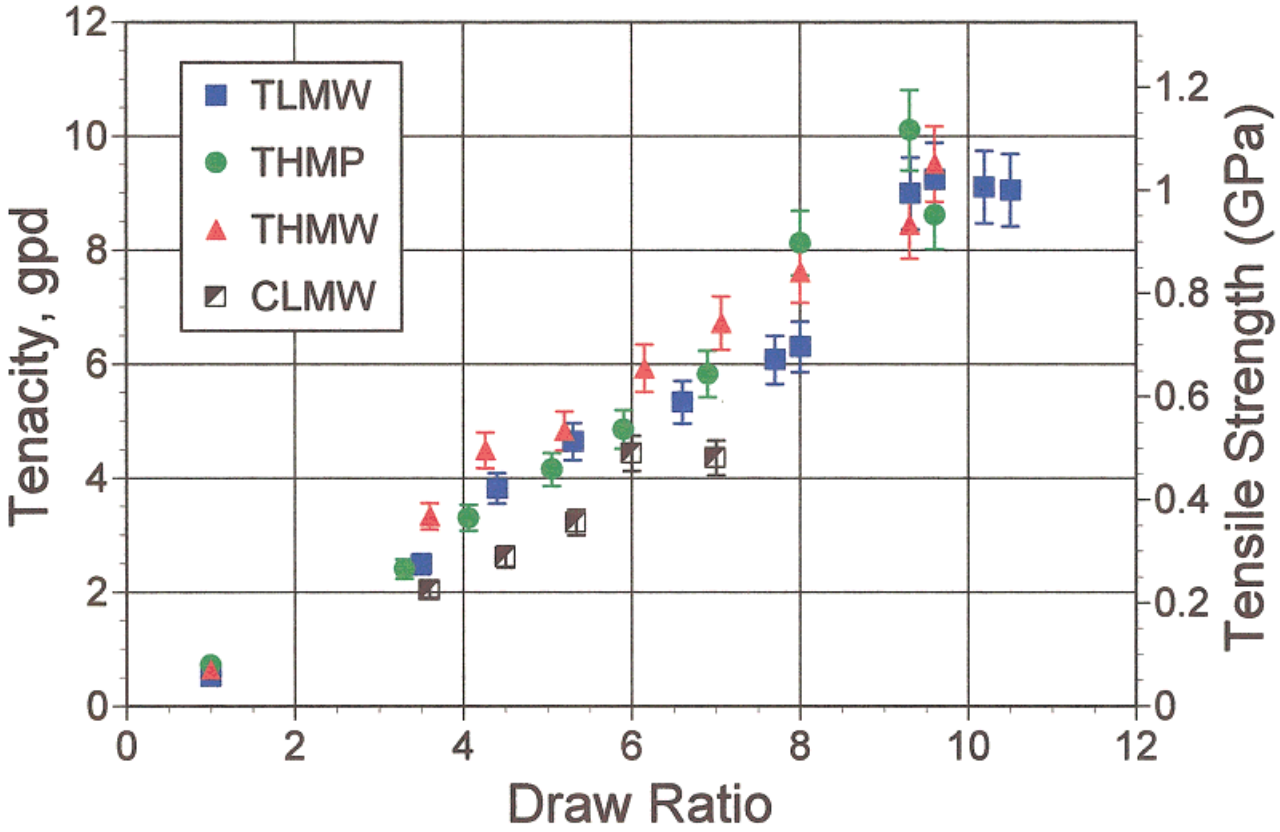

Figure 16 Tenacity or tensile strength as a function of draw ratio for aliphatic polyketone fibers. Scale showing gpd is precise; the scale showing GPa is approximate because the relation between gpd and GPa depends on the density, i.e., crystallinity. An average crystallinity of 48% was assumed in erecting the GPa scale. [Color figure can be viewed in the online issue, which is available at www.interscience.wiley.com.]

It appears that the general features of this transformation are the same for the aliphatic polyketones as were described in the earlier investigations. After this initial transformation from spherulitic to a microfibrillar morphology, the present data indicate that the microfibrils are further refined with the crystal dimensions perpendicular to the fiber axis continuing to decrease, but with little change in the long period and lamella thickness. Because the crystallinity increases with draw ratio, while crystal size is reduced, more crystals must be formed. We suggest that there are two processes occurring simultaneously. Crystals are being reduced in size by chain pullout at the boundaries of the microfibrils. These chains are elongated and oriented in the direction of the fiber axis producing a denser noncrystalline phase in the intermicrofibrillar region. Because this process is taking place at the draw temperature, there is sufficient thermal energy available to allow portions of these chains to undergo a "stress-induced recrystallization," resulting in the ultimate increase in the crystallinity. These new crystals would be expected to lie in the regions between the microfibrils produced by the original reorganization. This interpretation is somewhat similar to that proposed by Peterlin for polyethylene,[21,22] and has some of the characteristics of the model discussed by Taylor and Clark[18] to explain the elimination of the long period scattering in "superdrawn" polypropylene fibers. But it has greater similarities with the model discussed by Prevorsek et al.[23] for polyamide 6 fibers. In addition to the changes in the microfibril dimensions, the fibers develop voids that are elongated in the direction parallel to the fiber axis, and which presumably lie between the microfibrils. These voids are, perhaps, created by slipping of microfibrils past one another and opening of voids by the shearing action. A schematic model that describes these changes qualitatively is presented in Figure 15. The major dif-

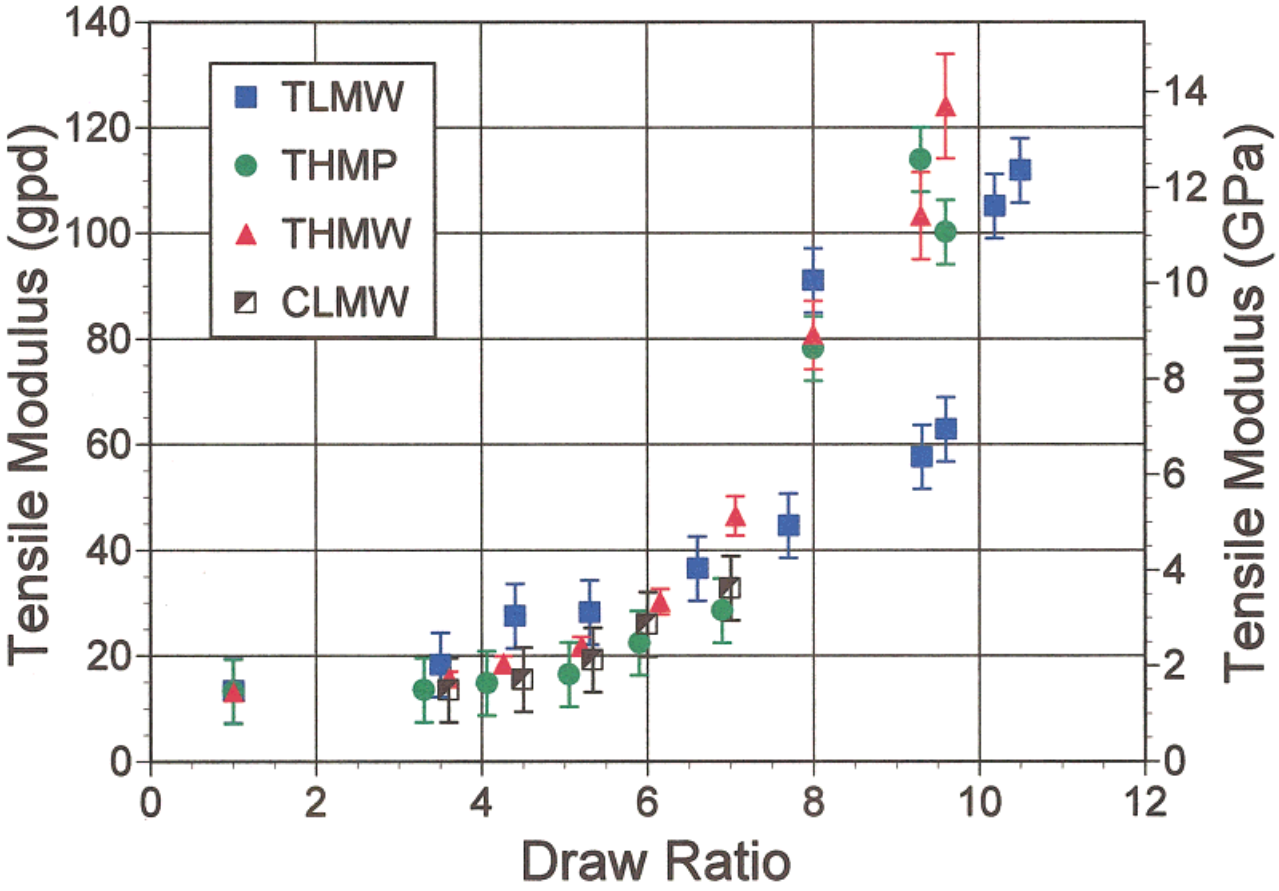

Figure 17 Tensile modulus as a function of draw ratio for aliphatic polyketone fibers. GPa scale erected as in Figure 16. [Color figure can be viewed in the online issue, which is available at www.interscience.wiley.com.]

ference between this model and that proposed by Prevorsek et al. for polyamide 6 is the addition of crystals formed by stress-induced recrystallization at the microfibril boundaries (i.e., in the intermicrofibrillar regions) and the creation of voids. Some aspects of this model are also fairly similar to the model used by Murthy et al.[24] in their treatment of the structure of drawn poly(ethylene terephthalate).

Tensile Mechanical Properties

Figure 16 shows the room temperature tenacity as a function of draw ratio for fibers produced from each of the four resins. The tenacity increases in an approximately linear fashion with draw ratio. The differences between the four resins appear to be relatively insignificant at a given draw ratio. But, because the terpolymers can be drawn to higher draw ratios than the copolymer, they also reach higher tenacities. Under the present drawing conditions the highest tenacities achieved were of order 10 gpd. This corresponds to a tensile strength of about 1.1GPa. Note that the data were taken in gpd units. Thus, the data plotted in Figure 16 was plotted in these units. The conversion of gpd to GPa involves the density of the filaments and, hence, the filament crystallinity. The GPa scale shown on the right side of Figure 16 (as well as Figs. 17 and 19) was erected by assuming a constant density corresponding to a crystallinity of 48%. Thus, the GPa scale slightly overestimates the tensile strength at low crystallinities and slightly underestimates it at high crystallinities. Nevertheless, this scale gives a good indication of strength of these filaments for those who prefer to think in terms of SI units.

The tensile elastic moduli of these fibers are plotted vs. draw ratio in Figure 17. The modulus also increases monotonically with draw ratio, but the increase is faster at high draw ratios than at

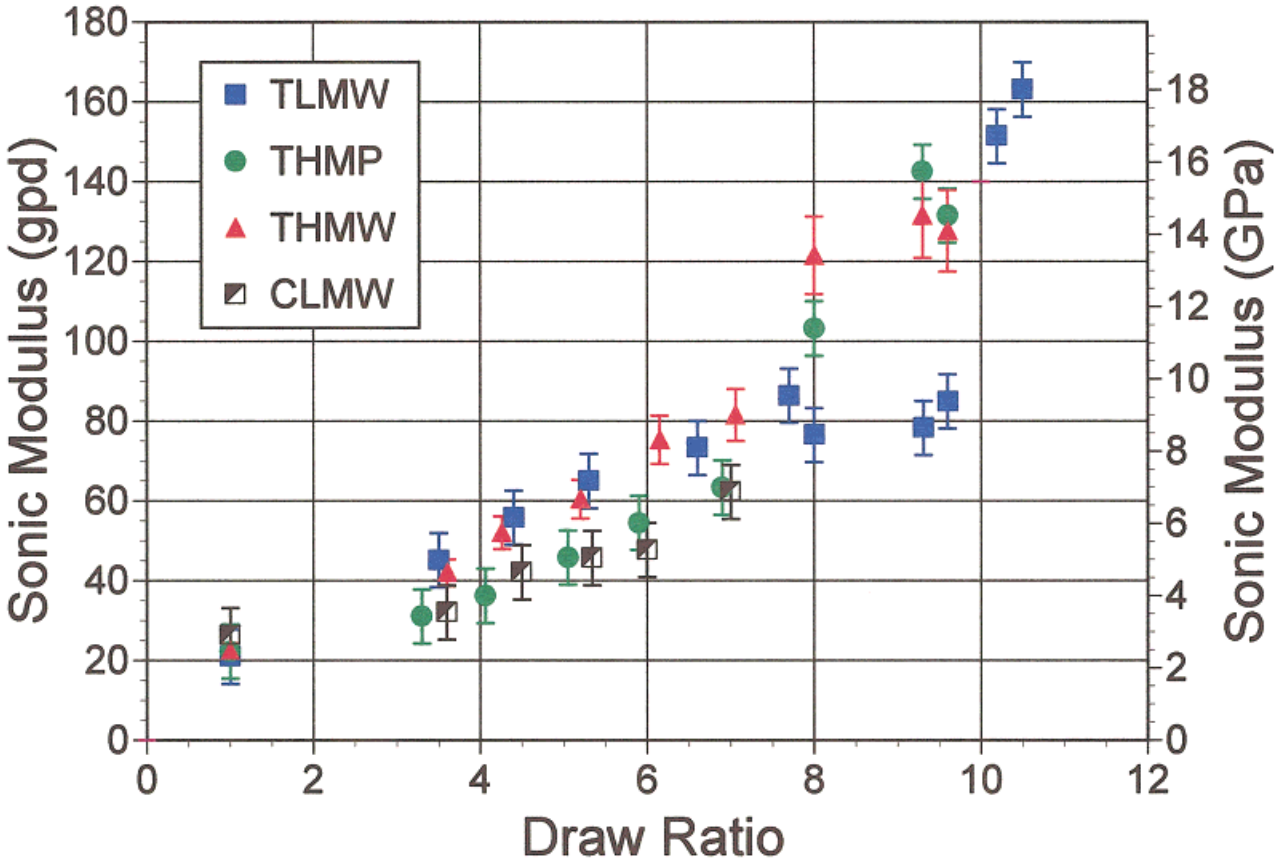

Figure 18 Sonic modulus vs. draw ratio for aliphatic polyketone fibers. [Color figure can be viewed in the online issue, which is available at www.interscience.wiley.com.]

low draw ratios. This suggests that the initial reorganization into the microfibrillar structure is complete at a draw ratio of about five times. Beyond five times the changes are associated with those described in the model above. The highest moduli achieved occur for fibers that have the highest molecular orientation and crystallinity, as expected. These values are of order 120 gpd (~13 GPa).

For comparison to the initial tensile modulus, the sonic modulus was also measured. Figure 18 shows the values obtained for the sonic modulus as a function of draw ratio. The trend is quite similar to that of the initial tensile modulus, but the values are somewhat higher. This is not surprising, as the two measurements do not measure the same quantity. The sonic modulus measures the fiber's response to a much higher frequency stimulus than does the tensile test. Thus, we might expect the value of the sonic modulus to be somewhat higher than the tensile modulus for a given sample.

The percent elongation to break is shown in Figure 19 for the drawn fibers. The elongation decreases with an increase in the draw ratio, but the values obtained at the highest draw ratios are still significant, indicating the basic ductile nature of these fibers.

The maximum strengths of these melt spun and drawn aliphatic polyketone fibers are similar to that of high-strength polyamide 66 and poly(ethylene terephthalate).[25] The maximum initial tensile moduli of the polyketone fibers appear to be a bit higher than either polyamide 66 or poly(ethylene terephthalate). Hence, the melt spun and drawn terpolymer fibers studied here exhibit tensile properties that make them candidates for applications as high-strength, high-modulus fibers. Still higher tensile strengths and moduli were achieved by Lommerts et al.[2] for the copolymer through the solution spinning and drawing technique. By this method they obtained tensile strengths as high as 3.8–3.9 GPa, and moduli as high as 50–55 GPa were achieved. This

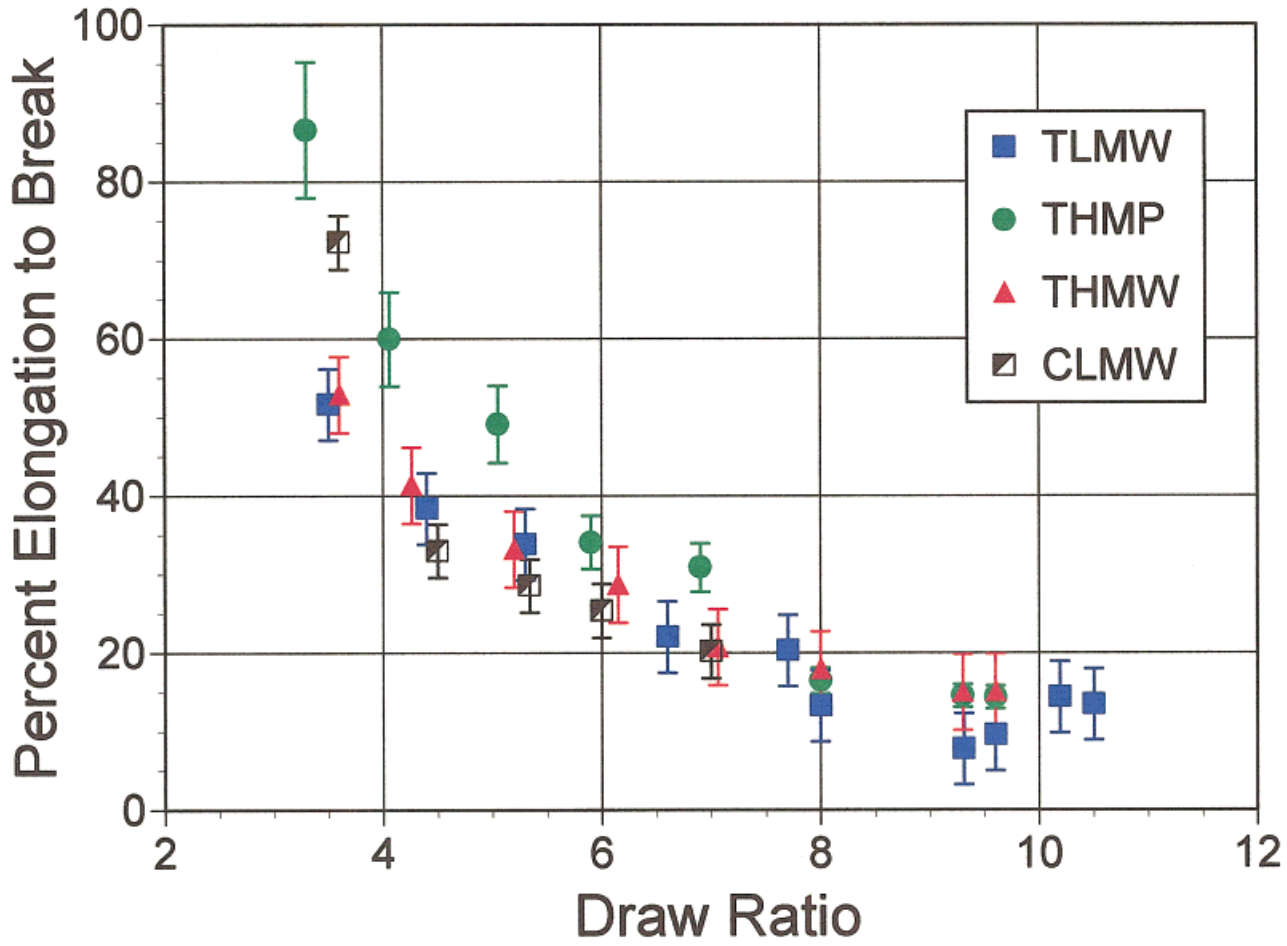

Figure 19 Percent elongation to break vs. draw ratio for aliphatic polyketone fibers. [Color figure can be viewed in the online issue, which is available at www.interscience.wiley.com.]

method of processing the fibers allows higher draw ratios to be obtained (26 for Lommerts) due to the disentangling effects of dissolving the polymer molecules in the solvent. It is also possible to use polymer with much higher molecular weight for solution spinning (300,000–420,000 g/mol for Lommerts). Both the higher draw ratios and higher molecular weight would be expected to result in higher tenacities and tensile moduli for the solution spun fibers. However, the advantages of melt spinning and drawing over the solution spinning technique are substantial, as no solvent handling is necessary. Thus, the melt spinning and drawing method described here is likely to be more economical than the solution spinning technique. Clearly, the fibers developed through melt spinning and drawing have sufficient strength and modulus for many applications. They also retain a large fraction of their strength at temperatures as high as 150°C. This fact will be the subject of a subsequent article. Further, we do not claim to have reached the maximum tensile strength and modulus that is potentially achievable from the aliphatic polyketone resins using melt spinning and drawing techniques. It may be possible, by further optimizing the composition, molecular weight, and the processing conditions to obtain aliphatic polyketone fibers with substantially higher properties than have been obtained in the present paper.

CONCLUSIONS

It was found that high-strength, high-modulus fibers could be produced from aliphatic polyketones by melt spinning and drawing. After melt spinning filaments with low orientation, it was

possible to continuously draw the terpolymers to draw ratios as high 10.5 times using a forced-air oven drawing process. Fibers drawn to these high draw ratios had tenacities as high as 10 gpd (~1.1 GPa) and tensile moduli as high as 120 gpd (~13 GPa). In the present experiments, we were unable to achieve copolymer fibers with such high draw ratios, tenacities, and tensile moduli. Possible explanations of this fact are that the high initial crystallinity of the copolymer or the high temperatures required to melt spin the copolymer resulted in filaments in which the drawability was limited by crosslinking or degradation. It was further found that these high strengths and moduli could not be achieved using a drawing technique in which the melt spun filaments are drawn after passing over heated rolls. At a given draw ratio, the tensile properties were little affected by termonomer composition and molecular weight, within the range studied.

The structures of the drawn fibers were characterized using WAXS, SAXS, birefringence, SEM, and thermal analysis (DSC). The drawn fibers developed high molecular orientation and exhibited a microfibrillar morphology that is similar, in many respects, to that of fibers produced from other semicrystalline polymers. In the present aliphatic polyketone fibers, the crystallinity and melting point can be controlled by adjustment of the termonomer (propylene) content. Fibers with melting point as high as 240°C, with the high maximum tensile properties described above, were produced from a resin containing about 3.5 mol % propylene.

The crystalline phase present in the terpolymer fibers of either composition was the β-phase under all conditions studied. The as-spun copolymer (CLMW) consisted largely of a β-phase, but the drawn copolymer was largely an α-phase at room temperature. This difference was attributed to a difference in the cooling rate of the melt spun and drawn filaments. The higher cooling rate of the melt spun filaments allowed much of the β-phase to be retained. The relatively slower cooling rate of the drawn fibers provided sufficient opportunity for the allotropic transformation from β to α-phase to occur. The unit cell dimensions of these phases were essentially identical to those reported by Lommerts et al.[3] and Klop et al.[4]

REFERENCES

1. Ash, C. E.; Waters, D. G.; Smaardijk, A. A. Proc Soc Plast Eng Annu Tech Conf 1995, XLI, 2319.
2. Lommerts, B. J.; ter Maat, H.; Huisman, R. Reproduced as Chapter 3 in a Ph.D. dissertation submitted by B.J. Lommerts , University of Groningen, October 1994.
3. Lommerts, B. J.; Klop, E. A.; Aerts, A. J Polym Sci B Polym Phys 1993, 31, 1319.
4. Klop, E. A.; Lommerts, B. J.; Veurink, J.; Aerts, J.; Van Puijenbroek, R. R. J Polym Sci B Polym Phys 1995, 1995, 33, 315.
5. Kormelink, H. G.; Vlug, M. A.; Flood, J. E. Chem Fibres Int 1999, 49.
6. Copeland, C. C.; M.S. Thesis, University of Tennessee, 1997.
7. Copeland, C. C.; Spruiell, J. E. Proc Soc Plast Eng Annu Tech Conf 1997, XLIII, 1800.
8. Stein, R. S.; Norris, F. H. J Polym Sci 1956, 21, 381.
9. Denbigh, K. G. Trans Faraday Soc 1940, 36, 936.
10. Bunn, C. W. Chemical Crystallography; Oxford University Press: London, 1961, p. 312.
11. Wilchinsky, Z. W. Advances in X-ray Analysis; Plenum Press: New York, 1963, p. 231, vol. 6.
12. Wignall, G.; Lin, J. S.; Spooner, S. J Appl Crystallogr 1990, 23, 241.
13. Flood, J. E.; Weinkauf, D. H.; Londa, M. Proc Soc Plast Eng Annu Tech Conf 1995, XLI, 2336.
14. Holt, G. A.; Spruiell, J. E. J Appl Polym Sci, submitted.
15. Samuels, R. J. Structurted Polymer Properties; John Wiley & Sons: Reading, NY, 1974.
16. Ash, C. E.; Flood, J. E. PMSE Preprints 1997, 76, 110.
17. Sze, G. M.; Spruiell, J. E.; White, J. L. J Appl Polym Sci 1976, 20, 1823.
18. Taylor, W. N.; Clark, E. S. Polym Eng Sci 1978, 18, 518.
19. Bodaghi, H.; Spruiell, J. E.; White, J. L. Int Polym Process 1988, III, 100.
20. Paluka, T.; Fischer, E. W. J Polym Sci B Polym Phys 1981, 19, 1705.
21. Peterlin, A. J Polym Sci Part C 1971, 13, 133.
22. Sakaoku, K.; Peterlin, A. J Polym Sci A-2 1971, 895.
23. Prevorsek, D. C.; Harget, P. J.; Sharma, P. K.; Reimschuessel, A. C. J Macromol Sci Phys 1973, B8, 127.
24. Murthy, N. S.; Grubb, D. T.; Zero, K.; Nelson, C. J.; Chen, G. J Appl Polym Sci 1998, 70, 2527.
25. Encyclopedia of Polymer Science; John Wiley & Sons: New York, 1988, p. 425, vol. 11; Ibid, p. 427.